

CROSS SHORE SANDBAR MIGRATION PREDICTED BY A TIME DOMAIN BOUSSINESQ MODEL INCORPORATING UNDERTOW

Wen Long¹, James T. Kirby² and T.-J. Hsu³

An existing Boussinesq wave model is modified to incorporate the contribution to undertow currents due to excess mass flux of surface roller. The model is then used to drive a sediment transport model and to predict both onshore sand bar migration events when wave skewness and asymmetry are dominating and offshore sand bar migration events when wave breaking introduced undertow prevails. The LIP11D experiments are examined to investigate both accretional and erosional cross-shore sediment transport processes.

INTRODUCTION

Long and Kirby (2003) have used Boussinesq model predictions to drive an instantaneous transport model, allowing morphology changes to accumulate on a wave by wave basis. Prompted by the work of Drake and Calantoni (2001) but using an instantaneous transport approach, Long and Kirby (2003) constructed an acceleration-dependent transport formula by including an explicit free stream fluid flow acceleration term into the Bagnold (1966) transport formula. Long and Kirby (2003) calibrated the model based on simulation of bar motion during the Duck '94 experiment during the week of September 23-30, 1994, and obtained quantitatively accurate representation of onshore bar movement events observed in the field which was also addressed by Hoefel and Elgar (2003) with similar success using data. The transport formula used in Long and Kirby (2003) has no specific mechanical underpinning. In order to develop a more appropriate, mechanically-based model, Long et al. (2004) resolved local wave boundary layer structure integrated with the Boussinesq model to give instantaneous prediction of bottom shear stress. The model is successful in predicting the onshore bar movements of Duck '94 experiment quantitatively.

The previous time domain Boussinesq model of Long et al (2004) underpredicts undertow current under strongly energetic wave breaking conditions. Hence both Long and Kirby (2003) and Long et al. (2004) are not able to predict offshore bar migration events. In the present study, we modify the existing Boussinesq model to incorporate the contribution to undertow currents due to excess mass flux of surface roller. We use the modified Boussinesq model to predict both onshore sand bar migration events when wave skewness

¹ Univ. of Maryland Center for Environmental Science, Cambridge, MD, 21613, USA, Email: wenlong@hpl.umces.edu

² Center for Applied Coastal Research, Univ. of Delaware Newark, DE, 19716, USA, Email: kirby@coastal.udel.edu

³ Dept. of Civil and Coastal Engineering, Univ. of Florida, FL, USA, Email: thsu@coastal.ufl.edu

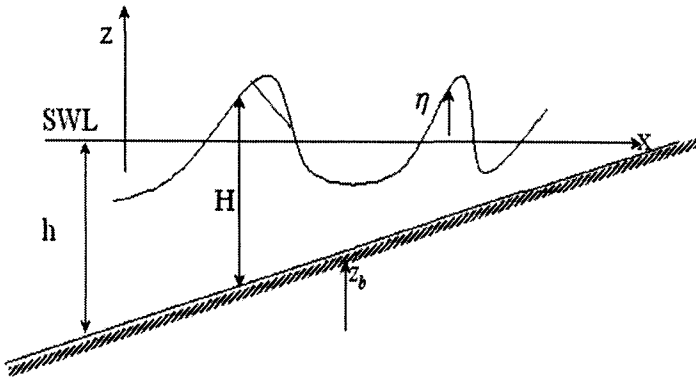


FIG. 1. Spilling breaker roller

and asymmetry are dominating and offshore sand bar migration events when wave breaking introduced undertow is dominating. The LIP11D experiments are examined in detail to investigate both accretional and erosional sediment transport processes.

MODIFIED BOUSSINESQ WAVE MODEL TO INCORPORATE UNDERTOW

In this research, we try to predict instantaneous near-bottom velocity with undertow automatically included. We use a roller model for description of breakers and include the impact of the roller in the mass conservation and momentum equations for the underlying water column. Figure 1 shows a schematic picture of spilling breaker with a conceptual roller (Schäffer et al., 1993). The fluid velocity is split into a wave component (irrotational) and roller (rotational) component. The following notations are used: $z_b = -h$ is bedlevel, η is the free surface elevation, r is the thickness of roller, $u(x, z, t)$ is the fluid velocity. The horizontal velocity is split into a wave component (irrotational) $u_w(x, z, t)$ including undertow and a roller component (rotational) u_r . The vertical velocity is assumed to have only a wave component (irrotational) meaning that vertical component of rotational flow is assumed to be small relative to irrotational flow. In general, the decomposition can be written as

$$\mathbf{u} = \mathbf{u}_w + \mathbf{u}_r \quad (1)$$

$$w = w_r + w_w \quad (2)$$

with

$$\mathbf{u}_r = \mathbf{C} - \mathbf{u}_w, \quad \eta - r \leq z \leq \eta; \mathbf{C} \approx \sqrt{gh}\mathbf{n} \quad (3)$$

where \mathbf{C} is the wave speed vector and \mathbf{n} is the wave direction unit vector $\mathbf{n} = (n_1, n_2)$. Here, we further assume

$$w_r = 0 \quad (4)$$

Hydrodynamic pressure $p(x, y, z, t)$ is assumed to be only determined by vertical momentum equation when $\mathbf{u}_r = 0$, i.e., assume that \mathbf{u}_r does not affect pressure. Irrotational velocity \mathbf{u}_w can be expressed as a 2nd order polynomial function of z in terms of representative levels: alpha level $\mathbf{u}_{w\alpha}$ and beta level $\mathbf{u}_{w\beta}$, where

$$\mathbf{u}_{w\alpha} = \mathbf{u}_w(x, t, z = z_\alpha); \mathbf{u}_{w\beta} = \mathbf{u}_w(x, t, z = z_\beta) \tag{5}$$

with

$$z_\alpha = \rho_1 h + \beta_1 \eta; z_\beta = \rho_2 h + \beta_2 \eta. \tag{6}$$

A new dependent variable is defined as

$$\tilde{\mathbf{u}} \equiv \beta \mathbf{u}_{w\alpha} + (1 - \beta) \mathbf{u}_{w\beta}. \tag{7}$$

When $\beta = 1$, equation (7) recovers Nwogu (1993) representation. (7) is used as dependent velocity. Kennedy et al. (2001) uses (6) with $\beta_1, \beta_2 \neq 0$ to improve representation of second harmonics in regular wave trains. We can express the velocity (\mathbf{u}_w, w_w) in terms of $\tilde{\mathbf{u}}$ as

$$\mathbf{u}_w = \tilde{\mathbf{u}} + (Ah - \xi) \nabla[\nabla \cdot (h\tilde{\mathbf{u}})] + \left(\frac{B-2A}{2} h^2 - \frac{\xi^2}{2} + h\xi\right) \nabla(\nabla \cdot \tilde{\mathbf{u}}) \tag{8}$$

$$w_w(x, y, z, t) = -\nabla \cdot (\xi \tilde{\mathbf{u}}) \tag{9}$$

where $\xi = h + z$ is distance above the bed,

$$A = \frac{1}{h} [\beta(h + z_\alpha) + (1 - \beta)(h + z_\beta)] \tag{10}$$

$$B = \frac{1}{h^2} [\beta(h + z_\alpha)^2 + (1 - \beta)(h + z_\beta)^2]. \tag{11}$$

The Euler equations in 3-D are integrated over the depth to obtain the following Boussinesq equations

$$\frac{\partial \eta}{\partial t} + \nabla \cdot \mathbf{M}_w + \nabla \cdot \mathbf{M}_r = 0 \tag{12}$$

$$\begin{aligned} & \frac{\partial \mathbf{M}_w}{\partial t} + \frac{\partial \mathbf{M}_r}{\partial t} + \nabla \cdot \left[\frac{\mathbf{M}_w \mathbf{M}_w}{H} + \frac{\mathbf{C} \mathbf{C} r^2 - \mathbf{M}_{wr} \mathbf{M}_{wr}}{r} \right] \\ & + \nabla \left[\frac{H^2}{2} - H^2 \left\{ [F_{23t} + \left(\frac{2H}{3} - h\right) F_{22t}] + \tilde{\mathbf{u}} \cdot [\nabla F_{23} + \left(\frac{2H}{3} - h\right) \nabla F_{22}] \right\} \right] \\ & - \nabla h [H - 2H \left\{ [F_{23t} + \left(\frac{H}{2} - h\right) F_{22t}] + \tilde{\mathbf{u}} \cdot [\nabla F_{23} + \left(\frac{H}{2} - h\right) \nabla F_{22}] \right\}] \\ & = 0 \end{aligned} \tag{13}$$

where

$$\mathbf{M}_w = H \tilde{\mathbf{u}} + H \left\{ (Ah - \frac{H}{2}) 2 \nabla F_{23} + (Bh^2 - \frac{H^2}{3} - 2Ah^2 + hH) \nabla F_{22} \right\} \tag{14}$$

$$M_r = \int_{-h}^{\eta-r} 0dz + \int_{\eta-r}^{\eta} (\mathbf{C} - \mathbf{u}_w)dz = (\mathbf{C} - \tilde{\mathbf{u}})r + O(\mu^2 r) \quad (15)$$

$$M_{wr} = \int_{\eta-r}^{\eta} \mathbf{u}_w dz = \tilde{\mathbf{u}}r + (\nabla F_{21} + 2\nabla h F_{22})(Ahr - \frac{H^2 - (H-r)^2}{2}) + (Bh^2 r - \frac{H^3 - (H-r)^3}{3})\nabla F_{22} \quad (16)$$

$$F_{21t} = \frac{\partial F_{21}}{\partial t}; F_{22t} = \frac{\partial F_{22}}{\partial t} \quad (17)$$

$$F_{21} = \nabla h \cdot \tilde{\mathbf{u}}; F_{23} = \frac{1}{2}\nabla \cdot (h\tilde{\mathbf{u}}); F_{22} = \frac{1}{2}\nabla \cdot \tilde{\mathbf{u}}. \quad (18)$$

Equations (12) and (13) are the new Boussinesq equations. They are accurate to the second order in dispersion, and are written in terms of $\tilde{\mathbf{u}}$ which can recover Nwogu (1993), Wei et al. (1995) \mathbf{u}_α , Kennedy et al. (2001) moving level and Gobbi et al. (2000) multi-level reference velocities. Equation (13) includes the momentum balance effect of surface roller for spilling breakers.

CROSS-SHORE SEDIMENT TRANSPORT

In this research, two sets of sediment transport formulations are tested. Model A uses the coupled Boussinesq model and an time-dependent Bagnold sediment transport model based on the Boussinesq model predicted bottom velocity with the ad-hoc free stream acceleration term proposed by Long and Kirby (2003). Model B uses the coupled Boussinesq model and Meyer-Peter-Müller (1948) sediment transport model with bottom shear stress given by the wave boundary layer model for the wave-related transport rate and a Bailard (1981) formula for mean current related transport rate.

Model A: Ad-hoc Modifications to Bagnold (1966) and Bailard (1981)

Here we use the Bagnold formula to calculate the instantaneous transport rate. An acceleration term is added to the formula following the suggestion of Drake and Calantoni (2001) and Hoefel and Elgar (2003). The added term here does not correspond in a direct way to the acceleration skewness measure employed in Drake and Calantoni, since it based on instantaneous acceleration rather than a statistical moment. The extended formula is written as

$$i_{tot} = i_b + i_s + i_a = \rho C_f \frac{\epsilon_B}{\tan \phi} [|u_b|^2 u_b - \frac{\tan \beta}{\tan \phi} |u_b|^3] + \rho C_f \frac{\epsilon_S}{w_{fall}} [|u_b|^3 u_b - \frac{\epsilon_S \tan \beta}{w_{fall}} |u_b|^5] + g(\rho_s - \rho) K_a (|u_{b,t}| - u_{b,cr}) \text{sign}(u_{b,t}) \quad (19)$$

where i_b , i_s are immersed weight sediment transport rate for bed load and suspended load respectively, i_a is the acceleration contribution, ϕ is the internal

angle of friction, $\tan \beta$ is the slope of the bedlevel, C_f is friction coefficient, w_{fall} is the sediment fall velocity, u_b is the bottom velocity. ϵ_B and ϵ_S are effectiveness coefficients for bed load and suspended load. $u_{b,t}$ is the acceleration of instantaneous free stream velocity u_b , and $u_{b,tc}$ is a threshold value. i_{tot} is the total immersed weight sediment transport rate. K_a is an empirical dimensional coefficient. The last term is set to zero when $|u_{b,t}| - u_{b,tc} \leq 0$.

The total volumetric sediment transport rate $q_{tot}(x, t)$ is calculated as

$$q_{tot} = \frac{i_{tot}}{g(\rho_s - \rho)} \quad (20)$$

Model B: Meyer-Peter Müller Formula with Shear Stress from Boundary Layer Model

The extended Bailard formula described by equation (19) has no specific mechanical underpinning. Recently, using a small-scale two-phase sheet flow model, Hsu and Hanes (2004) demonstrated that the instantaneous sediment transport rate under unsteady free stream flow follows the instantaneous bed shear stress closely. Previous work such as Ribberink (1998) and Hsu et al. (2006) tried to estimate transport rate using instantaneous bed shear stress estimation through simple power laws, and their model accuracy relies strongly on the bed shear stress prediction. In the present work, we use a physics-based model for the local boundary layer structure over the vertical, integrated with the Boussinesq model in order to provide a morphology evolution model. The adopted total volumetric transport rate is calculated by

$$q_{tot} = q_w + q_c \quad (21)$$

where q_w corresponding to wave-related transport rate is driven by bottom wave boundary layer shear stress, q_c is associated with mean velocity outside of the wave boundary layer. q_w is calculated according to Meyer-Peter-Müller formula

$$\Psi = A(\theta - \theta_c)^b \quad (22)$$

$$\Psi = q_w / (d\sqrt{(s-1)gd}) \quad (23)$$

$$\theta = \tau_b / ((\rho_s - \rho)gd) \quad (24)$$

where Ψ is the normalized transport rate, θ is the Shields parameter, θ_c is the threshold value of the Shields parameter for initiation of sediment transport, A and b are dimensionless constants, with typical values $A = 11$ and $b = 1.65$ (Ribberink 1998). τ_b is the instantaneous bed shear stress obtained from the wave boundary layer instead of using quadratic correlations. q_c is calculated according to the Bailard (1981) formula for mean current.

$$q_c = \frac{\rho}{g(\rho_s - \rho)} C_f \frac{\epsilon_B}{\tan \phi} [|u_b|^2 \bar{u}_b - \frac{\tan \beta}{\tan \phi} |u_b|^3] + \frac{\rho}{g(\rho_s - \rho)} C_f \frac{\epsilon_S}{w_{fall}} [|u_b|^3 \bar{u}_b - \frac{\epsilon_S \tan \beta}{w_{fall}} |u_b|^5] \quad (25)$$

Test	H_{m0} (m)	T_p (s)	D50(mm)	Wave Type	Duration(hr)
Test 1c	0.6	8.0	0.2	irregular	13
Test 1b	1.4	5.0	0.2	irregular	18

TABLE 1. Test conditions of LIP11D experiment

where \bar{u}_b is the mean bottom velocity based on a time average of instantaneous bottom velocity for an appropriate period of time.

Free stream velocity and pressure

The bottom boundary layer flow is driven by the free stream flow velocity and pressure gradient. The free stream velocity u_b , w_b and pressure p_b can be expressed as

$$u_b = \tilde{u} + \{Ah(\nabla F_{21} + 2\nabla h F_{22}) + Bh^2 \nabla F_{22}\} \quad (26)$$

$$w_b(x, y, t) = -F_{21} \quad (27)$$

$$p_b(x, y, t) = p_a + \rho g H - \rho \{H F_{21t} + H^2 F_{22t} + \tilde{u} \cdot [\nabla F_{21} H + \nabla F_{22} H^2 + 2F_{22} \nabla h H]\} \quad (28)$$

The wave bottom boundary layer structure is solved following Hsu et al (2006) and Long and Kirby (2004) to obtain the bottom shear stress τ_b with new improvements of using an implicit numerical scheme to save computation time.

MODEL TESTS WITH LIP11D EXPERIMENTS

Layout of the experiments and wave conditions

The LIP11D experiments were carried out with the purpose of obtaining detailed measurements of hydrodynamics and sediment transport in the surf zone. The experimental facility is the Delft Hydraulics' Delta Flume shown in figure 2. The flume is about 220 meters long, with a deep end of 4 meters still water depth. A plane beach starts at 20 meters from the wave paddles on the left. The test conditions are listed in table 1, where H_{m0} is the spectral estimate of significant wave height, T_p is peak wave period, D_{50} is median sand diameter. Test 1b is a strongly breaking wave condition case and the profile is eroded. Test 1c is a moderate wave condition case and the profile is accreted.

Model data comparison of waves and currents

During both Test 1b and Test 1c, 10 pressure gages are mounted at $x = 20m, 65m, 100m, 115m, 130m, 138m, 145m, 152m, 160m$ and $170m$ to measure the instantaneous pressure fluctuations, and the free surface elevation is inferred from these pressure measurements. We show the model data comparisons of the significant wave height H_{m0} and setup for wavehour 9 of Test 1b (test code #1b0909) and wavehour 7 of Test 1c (test code #1c0706). In addition to the

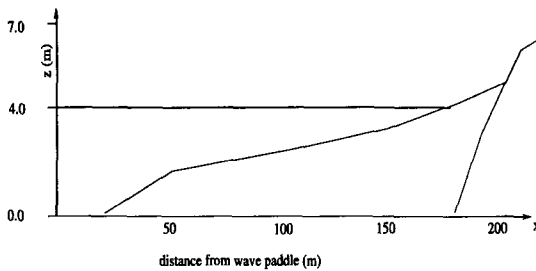


FIG. 2. Schematic layout of the LIP11D experiments

model wave height and setup validation, the vertical structure of the mean current is collected through 4 different wavehour model tests for Test 1c and Test 1b separately. The vertical profiles of velocities were measured by an array of EMF current meters mounted on a carriage towed to different x locations at different wavehours.

The modeled wave height and setup are compared to measured data for Test 1b in figure 3. Results for Test 1c are similar. The model results match with the measured data very well except near the numerical wave maker due to cutoff of high frequency energy (see Long, 2006). For Test 1b, waves break from the toe of the beach and wave height decreases monotonically from $x = 20m$ to $x = 180m$. The maximum wave setup is about $5cm$. For Test 1c, waves are smaller, and wave shoaling dominated the process from offshore to the crest of the sand bar. Further inshore of the bar crest, waves break and are dissipated rapidly. The maximum wave setup is about $3cm$.

The modeled mean flow results for Test 1b are shown in comparison with data in figure 4. Undertow currents are small for Test 1c (less than $0.15m/s$) and are not displayed. The undertow currents are stronger for Test 1b (maximum value is about $0.3m/s$). The model assumes a vertically constant return flow. The measurements show a large variation over the depth at $x = 138m$ and $x = 145m$ where waves break strongly. Hence the predicted value is much less than the measured maximum value that occurs near the bottom. For the Test 1b wavehour 17 (testcode #1b1706), at $x = 138m$, the upper most EMF current gage is out of water, and no measured and modeled data are plotted. The second EMF current gage is slightly below wave trough. Visual inspection of figure 4 shows that vertical integration of measured undertow is about $0.3m/s \times 0.7m/2 = 0.105m^2/s$, and the vertical integration of modeled undertow is about $0.17m/s \times 0.7m = 0.119m^2/s$. This indicates that although the model does not correctly predict the vertical structure of the undertow currents, it gives the overall return flow mass flux close to the measurements. For $x = 145m$ of Test 1b wavehour 7 (testcode #1b0707), the upper most EMF current gage is above the wave trough level, but not totally out of water, and it picks up onshore surface

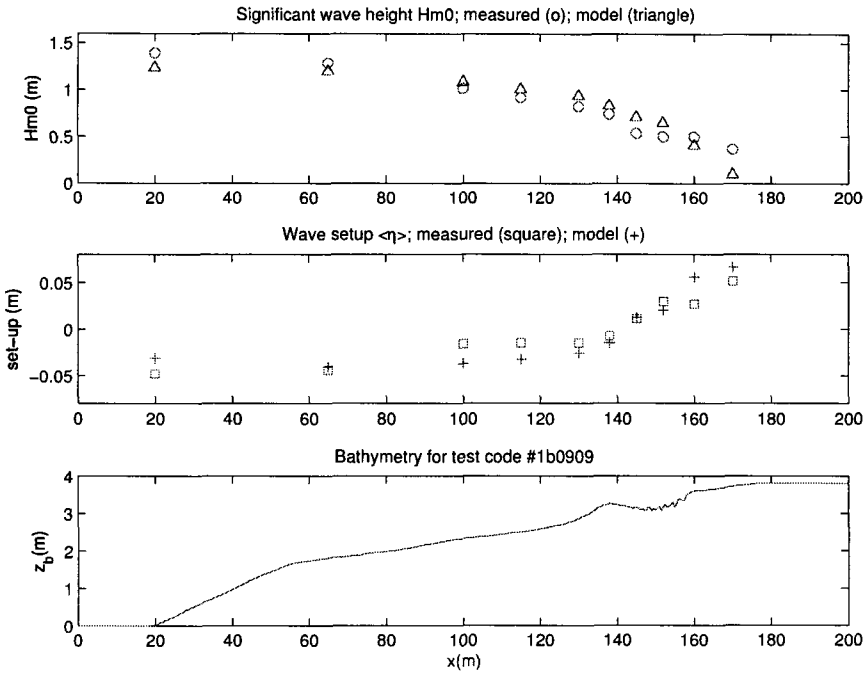


FIG. 3. Model data comparison of wave height and setup for Test 1b

currents due to wave breaking and wave skewness. The same visual inspection also indicates that the model predicts correct return flow mass flux. For Test 1c wavehour 7 (testcode #1c0706), the beach is accreted and the bar crest is higher compared to Test 1b, and at $x = 138m$, which is at the bar crest location, the first EMF current gage is totally above waves, and the second EMF gage (0.7m from the bottom) is close to mean water level, and it picks up the onshore surface current as well. For Test 1c wavehour 8 (testcode #1c0807), the first EMF gage is also out of water level, and there are no measured and modeled data.

Sediment transport and bar migration

During the Test 1b experiments, a wave gage WHM03 was placed at the toe of the slope $x = 20m$ and the surface elevation history was continuously recorded with a sampling frequency of 10Hz from wavehour 7 to wavehour 17. Hence, here we choose to model the hydrodynamics and the bathymetry change from wave hour 7 to wave hour 17 with both sediment model A and model B. The simulation parameters of waves for both model A and model B are set as: time step for waves $\Delta t = 0.025s$, spatial step $\Delta x = 0.5m$. For model A sediment transport, the bottom friction coefficient $C_f = 0.003$, bedload effectiveness $\epsilon_B = 0.135$,

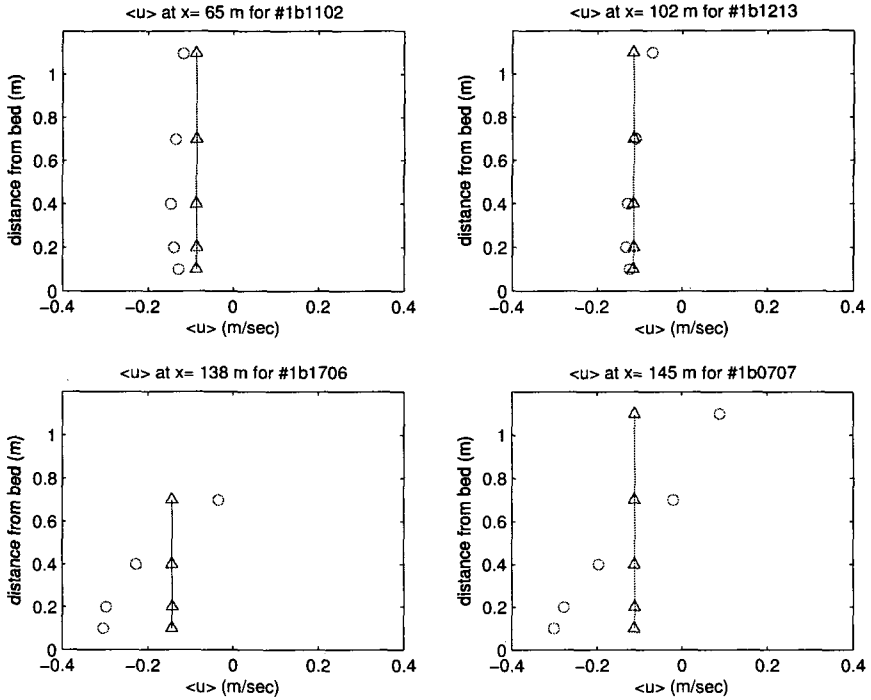


FIG. 4. Model data comparison of the vertical structure of undertow for Test 1b; data (o); model (Δ)

suspended load effectiveness $\epsilon_S = 0.010$, bed porosity $n_p = 0.4$, sediment internal friction angle $\phi = 32^\circ$, sediment median diameter $d_{50} = 0.2\text{mm}$, terminal velocity $w_{fall} = 2\text{cm/s}$, sediment density $\rho_s = 2650\text{kg/m}^3$, water density $\rho = 1000\text{kg/m}^3$, water molecular viscosity $\nu = 1.0 \times 10^{-6}\text{m}^2/\text{s}$. The acceleration term coefficient is $K_a = 0.0002\text{ms}$, and the critical acceleration threshold is $u_{bcr} = 0.5\text{m/s}^2$. For mode B sediment transport, the 1DV linear bottom boundary layer model is used to obtain bottom shear stress τ_b (Long et al. 2004). The bedlevel is updated every 448 seconds. The undertow current \bar{u}_b for the calculation of q_c is also by a time average of near bed velocity $u_b(x, t)$ over a period of 448 seconds.

The bedlevel predicted at the end of wavehour 17 by model A is shown along with the measured bedlevel in figure 5. In the figure panel (a), the modeled bedlevel is simulated using the full formula by (19). In the figure panel (b), the modeled bedlevel is due to the Bagnold formula. In the figure panel (c), the modeled bedlevel is due to the acceleration term solely. From the figure, we see that the measured bedlevels show a pronounced offshore bar movement

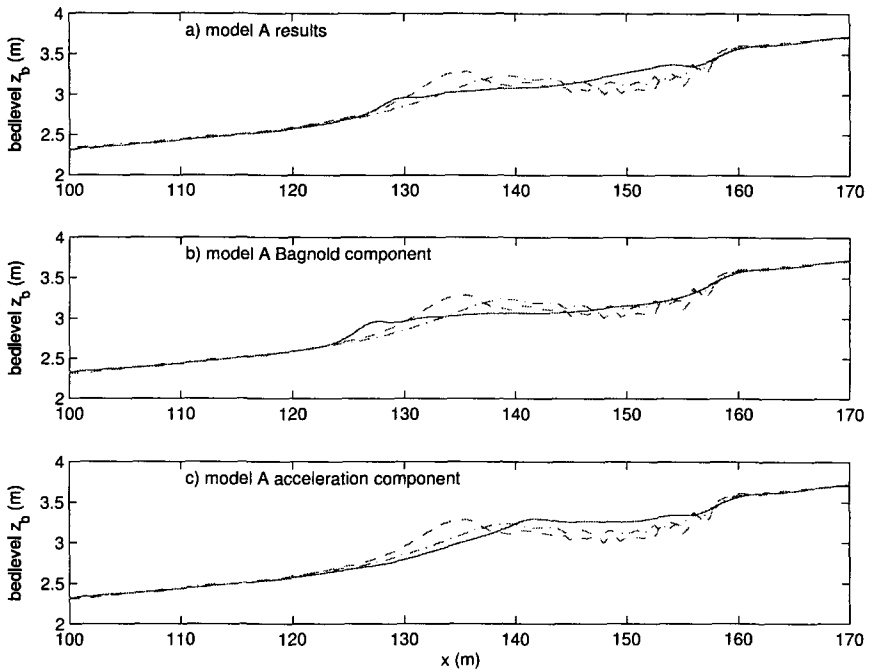


FIG. 5. Bedlevel change by model A for test 1b; (a) bedlevel due to both Bagnold formula and acceleration term; (b) bedlevel due to Bagnold formula; (c) bedlevel due to acceleration term; model bedlevel (solid line); measured initial bedlevel (dash-dotted line); measured final bedlevel (dash line)

with the bar crest height increased slightly. The modeled results due to the Bagnold component show a larger distance of offshore bar migration compared to measurements and the bar height is also decreased. On the other hand, the modeled results due to the acceleration component give slight onshore bar movement. The overall model A by both the Bagnold formula and the ad hoc acceleration term gives offshore bar migration for the bar and also accretion further inshore of the bar trough. The model gives qualitative agreement of the bar migration, but the quantitative comparison is poor.

The model B results are shown in figure 6. Here, the transport rate consists of a wave-related component q_w by Meyer-Peter-Müller formula and a current-related component q_c by Bailard (1981) as is described in (21). In figure 6, panel (a) shows the overall prediction, panel (b) shows the prediction due to q_w and panel (c) shows the prediction due to q_c . The results show that the q_w gives offshore movement of the bar and also some accretion further inshore of the bar trough. The current-related transport q_c gives small magnitude of offshore bar movement. The overall results are similar to model A, namely, offshore

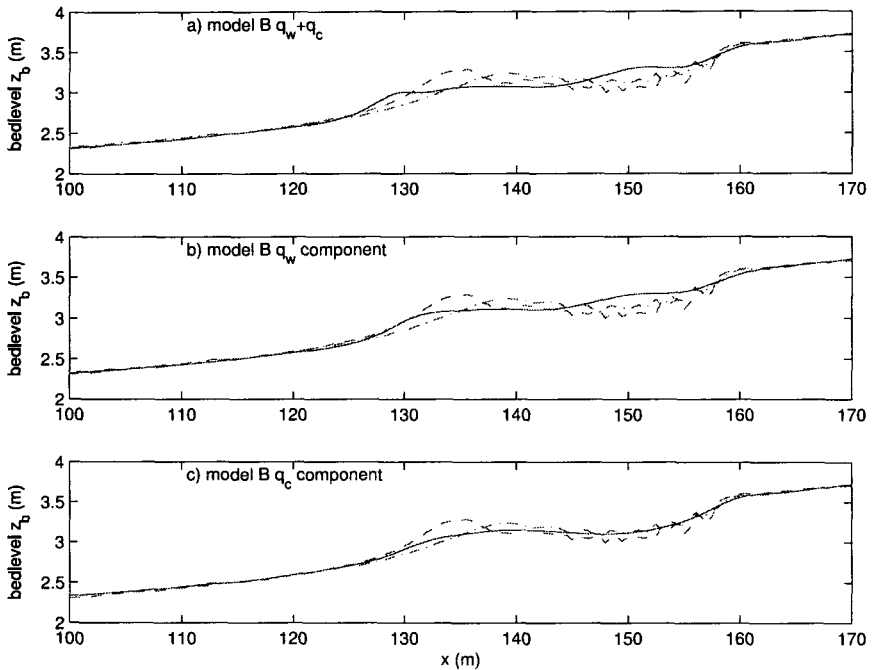


FIG. 6. Bedlevel change by model B for test 1b; (a) bedlevel due to both q_w and q_c ; (b) bedlevel due to q_w ; (c) bedlevel due to q_c ; model bedlevel (solid line); measured initial bedlevel (dash-dotted line); measured final bedlevel (dash line)

bar migration is predicted, inshore bar trough accretion appears in contrast to measured bathymetry and the bar crest height is underestimated.

For the Test 1c experiments, a wave gage WHM01 was placed at the toe of the slope $x = 20m$ and the surface elevation history was recorded with a sampling frequency of $10Hz$ from wavehour 1 to wave hour 10. This data series can be used as the input for the numerical wavemaker in Boussinesq model. Hence, here we choose to model the hydrodynamics and the bathymetry change from wave hour 1 to wave hour 10.

The simulation parameters both model A and model B are set similar to Test 1b except that here the bottom friction coefficient $C_f = 0.001$ with less turbulent intensity for smaller wave height compared to Test 1b, the acceleration term coefficient $K_a = 0.0004ms$, with the critical acceleration threshold $u_{bter} = 0.3m/s^2$. The bedlevel is updated also every 448 seconds. The undertow current \bar{u}_b for the calculation of q_c is again obtained by a time average of near bed velocity $u_b(x, t)$ over a period of 448 seconds.

The model A results are not shown here due to space limitations. The measurements show onshore migration of the sandbar with a increased bar height.

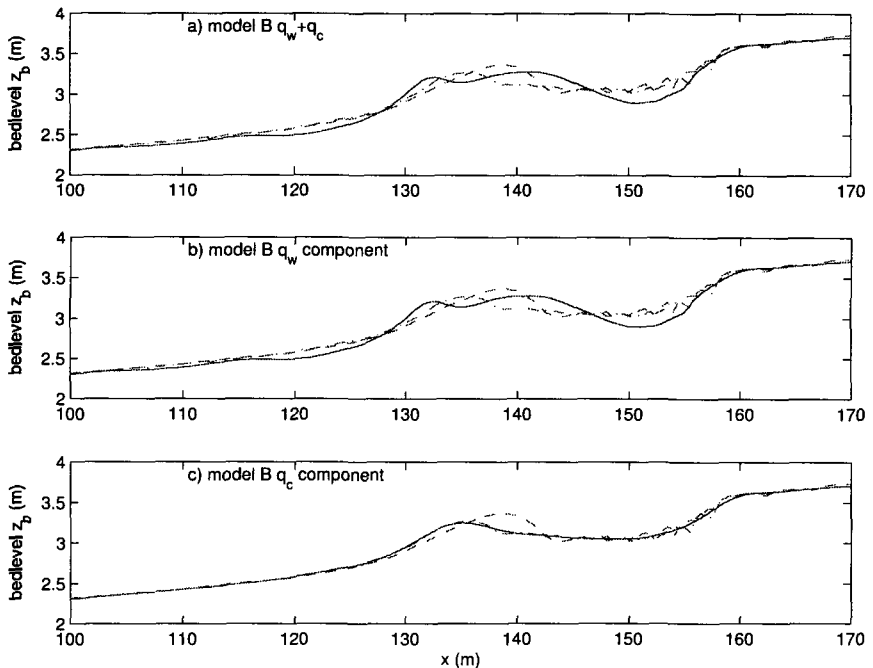


FIG. 7. Bedlevel change by model B for test 1c; (a) bedlevel due to both q_w and q_c ; (b) bedlevel due to q_w ; (c) bedlevel due to q_c ; model bedlevel (solid line); measured initial bedlevel (dash-dotted line); measured final bedlevel (dash line)

The Bagnold formula gives almost no change to the bedlevel, while the transport due to the acceleration term gives correct bar movement direction and distance. The overall results show accretional onshore bar movement. Again, the bar crest height is underestimated by the model.

The model B results are shown in Figure 7. Similar to the results of model A, the current-related component predicted by the Bailard formula in panel (c) shows no effect on bathymetry. But the q_w predicted by the Meyer-Peter-Müller formula and the wave boundary layer model shows accretion of the beach profile at the offshore side of the sand bar. There is also some erosion further inshore of the bar trough which results in an increase of the bar crest height. The onshore bar migration event is predicted but the scene is more complicated than the measurements.

CONCLUSIONS

A cross shore sediment model is built based a new Boussinesq model with undertow incorporated and two different instantaneous sediment transport formulas. The sediment model is then tested with LIP11D experiments for both

accretional and erosional bar migrations. The model predicts the onshore bar migration events qualitatively well. For offshore bar migrations, model success is limited due to lack of mechanism to account for vertical structure of undertow near bed in the model.

ACKNOWLEDGMENTS

This research was supported by the National Ocean Partnership Program and the Office of Naval Research, Coastal Geosciences Program.

REFERENCES

- [1] Drake, T. G. and J. Calantoni, Discrete particle model for sheet flow sediment transport in the nearshore, *J. Geophysical Research*, **106**, C9, pp 19,859-19,868, 2001
- [2] Gobbi, M. F., J. T. Kirby and G. Wei, A fully nonlinear Boussinesq model for surface waves. II. Extension to $O(kh^4)$, *Journal of Fluid Mechanics*, **405**, pp 181-210, 2000
- [3] Hoefel, F. and S. Elgar, Wave-induced sediment transport and sandbar migration, *Science*, **299**, 1885-1887, 2003
- [4] Hsu, T.-J. and D. M. Hanes, The effect of wave shape on sheet flow sediment transport, *J. Geophysical Research*, **109**, C06025, doi:10.1029/2003JC002075, 2004
- [5] Hsu, T.-J., Elgar, S., Guza R. T. Wave-induced sediment transport and onshore sandbar migration, *Coastal Engineering*, **53**, pp817-824, 2006.
- [6] Long, W. and J. T. Kirby, Cross-shore sediment transport model based on the Boussinesq equations and an improved Bagnold formula, *Proceedings Coastal Sediments '03*, Clearwater Beach, May, 2003
- [7] Long, W., PhD Thesis, University of Delaware, 2006.
- [8] Kennedy, A. B., J. T. Kirby, Q. Chen, and R. A. Dalrymple, Boussinesq-type equations with improved nonlinear behaviour, *Wave Motion*, **33**, pp 225-243, 2001
- [9] Long, W., T.-J. Hsu and J. T. Kirby, Modeling cross-shore sediment transport processes with a time domain Boussinesq model, *Proceedings 29th International Conference on Coastal Engineering*, Lisbon, Sept., 2004
- [10] Nwogu, O. G., An alternative form of the Boussinesq equations for nearshore wave propagation, *J. Waterway, Port, Coast., Ocean Engrg*, **119(6)**, pp 618-638, 1993
- [11] Ribberink, J. S., Bed-load transport for steady flows and unsteady oscillatory flows, *Coastal Engineering*, **34**, pp59-82, 1998
- [12] Schäffer, H. A., P. A. Madsen and R. Deigaard, A Boussinesq model for waves breaking in shallow water, *Coastal Engineering*, **20**, pp 185-202, 1993
- [13] Wei, G., J. T. Kirby, S. T. Grilli and R. Subramanya, A fully nonlinear Boussinesq model for surface waves. I. Highly nonlinear, unsteady waves, *Journal of Fluid Mechanics*, **294**, pp 71-92, 1995